THESIS FOR THE DEGREE OF LICENTIATE OF ENGINEERING

Effect of Temperature on Mechanical Properties of Railway Wheel Steels

Dimitrios Nikas

Department of Materials and Manufacturing Technology
CHALMERS UNIVERSITY OF TECHNOLOGY
Gothenburg, Sweden, 2016

Effect of Temperature on Mechanical Properties of Railway Wheel Steels

Dimitrios Nikas

ISSN 1652-8891
No. 105/2016

Department of Materials and Manufacturing Technology
Chalmers University of Technology
SE-412 96 Gothenburg
Sweden
Tel.: +46 (0)31 772 1000

Printed by Chalmers Reproservice
Gothenburg, Sweden 2016

Effect of Temperature on Mechanical Properties of Railway Wheel Steels

Dimitrios Nikas

Department of Materials and Manufacturing Technology
Chalmers University of Technology

ABSTRACT

One of the most important aspects in railway operation is the interaction between rail and wheel. The contact conditions give rise to wear and damage in both components. Medium carbon steels are used in these components due to their combination of high strength and good wear properties in relation to cost. In service, high surface temperatures develop because of frictional heating on traction, braking, curving and occasional full slippage. Furthermore, long-term block braking may heat the wheel rim to over 500°C. It is thus relevant to examine the high temperature performance of wheel material as well as the decrease in strength after thermal exposure.

In the current thesis, two railway wheel steels are examined. These are the medium carbon steels UIC ER7T and ER8T (~0.55 wt.% C), heat-treated to a near pearlitic microstructure with some 5–10% pro-eutectoid ferrite in the wheel tread surface. Specimens were extracted from virgin wheels and pre-strained either monotonically or cyclically, to imitate plastic deformation developing in the wheel tread surface in service. Both un-deformed and pre-strained materials were heat treated at various temperatures from 250°C to 650°C for various time durations, and the change in room temperature hardness as measured before and after heat treatment was analysed. Samples were analysed using Scanning Electron Microscopy (SEM), to examine microstructure degradation. Additionally, Electron Backscatter Diffraction Analysis (EBSD) was used to evaluate if orientation gradients in the pearlitic colonies affect the spheroidisation of the pearlitic microstructure that is observed at higher temperatures.

Analyses after the room temperature hardness measurements showed that hardening due to strain ageing takes place at around 300°C while microstructural degradation caused softening at higher temperatures. Spheroidisation of the pearlite started to become visible at 450°C for the un-deformed material and at around 400°C for the pre-strained. The spheroidised areas appear to have lost their initial orientation gradients after spheroidisation and obtain a more uniform orientation.

Cyclic tests at elevated temperature revealed cyclic hardening at around 300°C, as an effect of dynamic strain ageing. At higher temperatures, cyclic softening followed due to a combination of increasing thermal activation and spheroidisation.

Keywords: Low cycle fatigue (LCF); Hardness; Thermal effects; Pearlitic wheel steels; EBSD; Spheroidisation;

PREFACE

This licentiate thesis is based on the work performed in the project MU28 within the National Centre of Excellence CHARMEC (Chalmers Railway Mechanics). The experimental work presented in this thesis is based on experiments that have been performed at the department of Materials and Manufacturing Technology at Chalmers University of Technology from August 2013 until March 2016. The project was carried out under the supervision of Docent Johan Ahlström.

The work upon which this thesis is based is described in more detail in the following, appended papers. The papers are:

Paper I: **Mechanical properties and fatigue behaviour of railway wheel steels as influenced by mechanical and thermal loadings**

D. Nikas, J. Ahlström, A. Malakizadi

Published in *Wear*, and presented at the *10th International Conference on Contact Mechanics and Wear of Rail/Wheel Systems* (CM2015), Colorado Springs, USA, 2015,

DOI: 10.1016/j.wear.2016.04.009

Paper II: **Characterization of microstructural changes in near pearlitic steels using orientation imaging microscopy - Influence of predeformation on local sensitivity to thermal degradation**

D. Nikas, J. Ahlström

Published in *IOP Conference Series: Materials Science and Engineering*,

DOI: 10.1088/1757-899X/89/1/012039

Papers not appended to the thesis:

Thermal deterioration of wheel steels

D. Nikas, J. Ahlström

Proceedings of the 35th Risø International symposium, Risø, Denmark, p. 411–420, 2014

High Temperature Tread Braking Simulations Employing Advanced Modelling of Wheel Materials

Ali Esmaeili, Tore Vernersson, Dimitrios Nikas, Magnus Ekh

Proceedings of the 11th International Heavy Haul Association conference, Perth, Australia, 2015

CONTENTS

1 Introduction

1.1 Background

One of the most important aspects in railway operation is the interaction between rail and wheel. If one takes into account that the contact patch between these two components is around the size of a small coin it is clear that very high loads act on a very small area and both rails and wheels encounter wear and damage. Frictional forces the surface caused by recurring acceleration, braking, curving and occasional full slippage can cause cyclic plastic deformation and heating which in turn causes an aligned, anisotropic microstructure with altered mechanical behaviour. Control of material property degradation is an important topic for guiding maintenance as well as ensuring safety of railways, since it will allow for a more accurate prediction of material wear and lifetime.

The railway industry still relies on steels for the manufacturing of wheels and rails. Medium carbon steels (~0.5 wt.% C) are used for the manufacturing of wheels due to their combination of high strength and good wear properties in relation to cost. Moreover, heat treatment procedures can give these wheel materials a near pearlitic microstructure, with finer pearlite closer to the wheel tread surface and favourable residual stress distribution. Rails are typically made from steels with slightly higher carbon content, heat treated to a fully pearlitic microstructure. Bainitic microstructures have been tried out for both wheel and rails and put into service, but still the pearlitic grades dominate strongly the market.

It is of critical importance to study the material microstructure and understand how it performs under a complex combination of mechanical and thermal loadings, and how this microstructure is affected by all the various factors that come into play in service. Understanding how railway materials behave is essential for materials selection for different environments, design of railway components and tuning of traction and braking systems. The sensitivity to degradation processes and crack formation is dependent on material and microstructure. The aim of this project is to help judge limits for utilisation of wheel and rail materials with respect to combined cyclic mechanical and thermal loadings.

1.2 Objectives

In this thesis, the deterioration of the mechanical properties of railway wheel steels after exposure to high temperatures and plastic deformation; specifically the medium carbon steels UIC ER7T and ER8T (~0.55 wt.% C) were examined. The high thermal loads in service can cause severe degradation of the material microstructure, more specifically spheroidisation of the pearlite, which combined with plastic deformation (that makes the material more prone to spheroidisation) can lead to severe deterioration of the material's mechanical properties.

The focus in this first part of the project was to quantify the changes in mechanical performance of near-pearlitic wheel steels exposed to combined mechanical and thermal loadings up to 650°C. This was done by first investigating the changes in room temperature hardness that are induced by thermal degradation with and without prior plastic deformation. A microstructural evaluation was made to correlate results from hardness testing with the microstructural degradation, and to examine microstructure variations with depth below the running surface. The elevated temperature performance was studied by low cycle fatigue testing. The study complements the literature about mechanical behaviour of near-pearlitic wheel steels exposed to combined thermal and mechanical loadings and provides a better understanding and quantification of how the

material properties will vary with depth below the wheel tread; an important issue since material at depth becomes exposed to surface loadings after wheel re-profiling during maintenance. EBSD was used in an attempt to evaluate the influence of orientation gradients (correlating with the dislocation density according to literature) on the degradation of microstructure, and to examine how it changes with increasing heat treatment temperature.

2 Theory

2.1 Railway wheels and operation conditions

Axle loads for passenger trains in Europe vary between 15–25 tonnes [1] and can go even higher when it comes to freight trains. A typical wheelset that should carry this load is shown in Fig. 2.1 (left). The contact patch for a standard profile rail and wheel (and 11 tonnes contact force) is elliptical with 18 x 11 mm for the major and minor axes of the ellipse [1]. When the wheel is worn, the shape becomes more circular. When the dynamic effects and tractive forces are added, one can understand that very high demands are put on the materials that are used for these components. Moreover, higher speed and load demands from the railway industry increase the requirements on the material quality of wheels and rails. Another important aspect of railway operation is regular maintenance. The service life of a wheel can vary between 300,000 and 2,500,000 km and during this lifetime two to five re-profilings are necessary to remove surface defects and small cracks that might have initiated. This procedure exposes new material on the surface of the wheel that has slightly different properties than the original surface [1]. Control of material property degradation in wheels is an important topic for guiding maintenance and ensuring safety of railways.

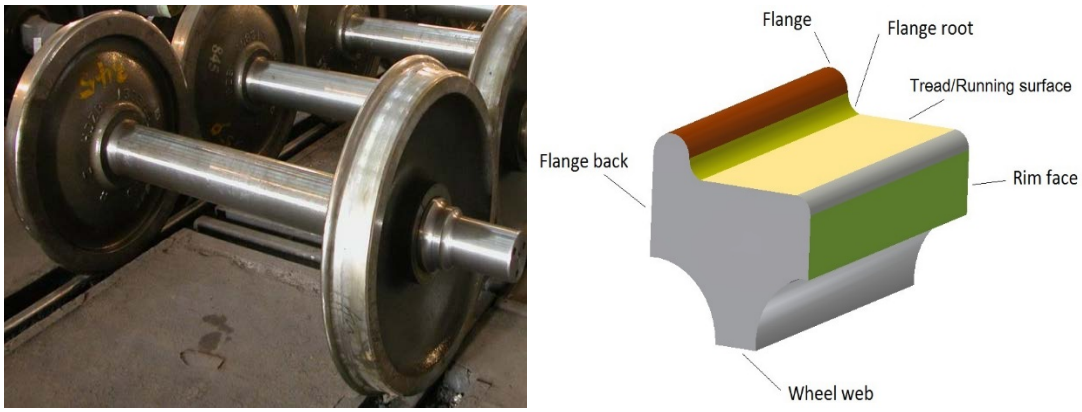

Fig. 2.1: A typical wheelset (left) and a sketch of a wheel rim cut-out from a railway wheel with relevant nomenclature (right).

The areas of the wheel that are affected the most during operation are the flange, the flange root and the tread (Fig. 2.1, right). Wear is the main issue for the flange and the flange root but for the tread, in addition to wear there is also rolling contact fatigue (RCF) loading and thermal loading coming from frictional heating. Frictional forces arise in the wheel-rail contact and in the case of block braking also in the contact between block and wheel. In practice temperatures over 500 °C can be achieved [2] during pronounced block braking. In the outermost millimetres of the wheel tread, the material also experiences large deformation and plastic flow due to creepage. This makes it prone to spheroidisation [3].

Even higher temperatures up to approximately 1050 °C can be reached on occasional slippage when the wheels skid along the rail for a short time [4], [5]. This causes phase transformations in the steel, often resulting in brittle martensitic patches on the wheel tread that can lead to spalling and other problems. Due to the volume change from this phase transformation residual compressive and tensile stresses are induced in the

material that make it prone to cracking when additional load is applied. Although traction control systems in passenger trains have improved in recent years, reducing thermal events, on freight trains that still operate on simpler designs and carry higher axle loads these phenomena are still present to an extent.

The following sections in this chapter will describe the microstructural related phenomena that occur in wheel material when exposed to medium high temperatures (250 – 650 °C).

2.2 Material microstructure

The most common wheel materials used for rolling stock today are medium carbon steels heat-treated to give a near-pearlitic microstructure close to the tread surface. Different standards and steel designations exist around the world, shown in table 2.1 [6],[7].

Table 2.1: Wheel materials used for rolling stock

Region	*Specification*	*Steel grade*	*Carbon content (%)*
Europe	EN13262	ER6	≤0.48
		ER7	≤0.52
		ER8	≤0.56
		ER9	≤0.60
North America	AAR M-107/M-208	Class L	≤0.47
		Class A	0.47–0.57
		Class B	0.57–0.67
		Class C	0.67–0.77
		Class D	
Japan	JIS E 5402-1	SSW QS	0.60–0.75
		SSW QR	
		SSW QRH	

Two grades are commonly used on trains in Europe; the ER7 grade is the dominant grade on freight trains and on many passenger coaches, while the ER8 grade with slightly higher carbon content is often used for passenger trains with driven wheels, so-called EMUs (Electric multiple units) [8]. In production, after forging and rolling, wheels are rim chilled; a heat treatment yielding a microstructure consisting of fine pearlite with some 5–10 vol. % pro-eutectoid ferrite just below the wheel tread [9]. After this heat treatment, the letter "T" is added to the designation so in this thesis the commonly used names R7T and R8T will be used.

2.2.1 Morphology and formation of pearlite

Pearlite is a two-phase structure formed during the transformation from austenite. It grows from nuclei that exist in the prior austenite grain boundaries [10]. These nodules grow until they finally meet with each other. Pearlite colonies that consist of alternating lamellas of ferrite and cementite (Fe_3C) exist within each nodule and have a single orientation (Fig. 2.2). In steels with hypo-eutectoid composition, free ferrite is also present in the microstructure.

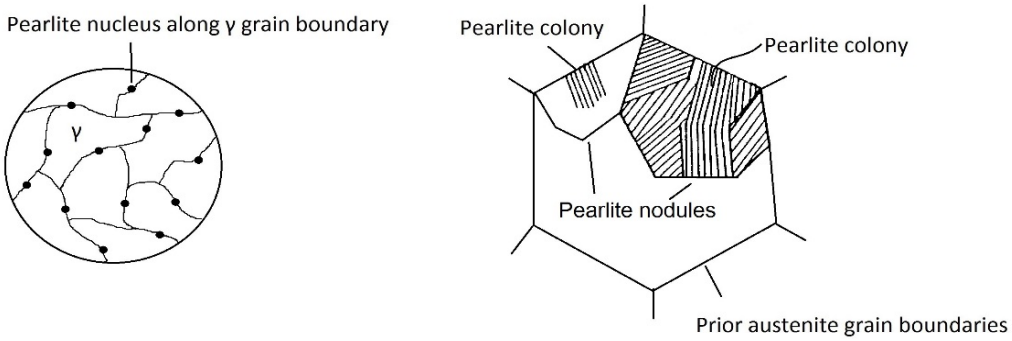

Fig. 2.2: Sketch of pearlite formation

The transformation temperature determines the resulting interlamellar spacing, controlled by the carbon diffusion rate. Thus, it can be manipulated using specific heat treatments depending on the chemical composition of the material. Heat treatments that employ rapid cooling have the ability to delay the transformation temperature to lower temperatures, which in turn results in larger volume fraction of pearlite (with slightly hypo-eutectoid composition) and a refined lamellar structure [11]. The nodule size is affected by the prior austenite grain size but has little effect on interlamellar spacing [12]. It was also shown that colonies within the same nodule have a similar interlamellar spacing [13].

2.2.2 Strength of pearlite

Increasing the carbon content increases the steel's strength, often at the expense of fracture toughness. More specifically for steels near the eutectoid composition with some free ferrite present, the interlamellar spacing is associated with controlling strength whereas the ferrite phase governs ductility [14]. Refinement of the interlamellar spacing limits the dislocation movement, which mainly occurs in the ferrite lamellas, and effectively increases the steels' strength. Refinement can be accomplished by lowering the transformation temperature (by controlling the cooling rate). The strength of both ferrite and pearlite follows a Hall-Petch type relationship:

$$\sigma_y = \sigma_0 + k_y S^{-\frac{1}{2}} \tag{1}$$

where S denotes the interlamellar spacing and σ_y is the yield stress. The material constants σ_o and k_y are used for the starting stress for dislocation movement and the strengthening coefficient (or dislocation locking) respectively [9],[15]. The yield strength of pearlite is mainly dependent on the interlamellar spacing and is independent of prior austenite grain size or nodule diameter [14].

Another interesting fact is that the dependency of interlamellar spacing on transformation temperature increases with the carbon content. In addition, the lower the carbon content of pearlite, the larger the interlamellar spacing, according to Bae et al.[16]. It was found that the carbon content is more influential than interlamellar spacing or prior austenite grain size when it comes to ductility.

When it comes to hypo-eutectoid steels it was reported [17] that the strength of pearlitic colonies didn't follow a Hall-Petch type relationship and varied even though the interlamellar spacing was kept constant. This was attributed to the influence of hydrostatic stresses due to the presence of the free ferrite phase.

A very important consideration when it comes to pearlitic steels is how the lamellar microstructure interacts with the dislocations when the material is subjected to external loadings, either monotonic or cyclic. The density of dislocations that are produced during cyclic loading is much higher than the amount that is produced at monotonic loading for similar stress levels. Moreover during a monotonic test reaching larger strains, slip planes are rotating towards the tensile axis which is not the case for fully reversed cyclic loading [18]. According to the model proposed by Miller-Smith [19], dislocations pile up on the interface between cementite and ferrite. Stress concentration then leads to the fracture of the cementite lamellas and plastic deformation continues in the neighbouring ferrite lamella. Strain localisation is happening only on a few glide planes.

Based on the above assumption that dislocation sources exist on the interface between cementite and ferrite in a local micro yield region, the yield strength of pearlite depends on the necessary stress to move dislocations in ferrite between two cementite walls, thus it increases with the refinement of the interlamellar spacing which in turn leads to strengthening of the material [20].

2.2.3 Pearlite spheroidisation

At exposure to medium temperatures, starting from around 400 °C up to around 750 °C, increasing microstructural degradation occurs. According to common heat treatment practice, depicted within a binary iron-carbon phase diagram (Fig 2.3), for temperatures below the α-γ transformation line (A_{C1}) there exists a zone where spheroidisation starts to occur.

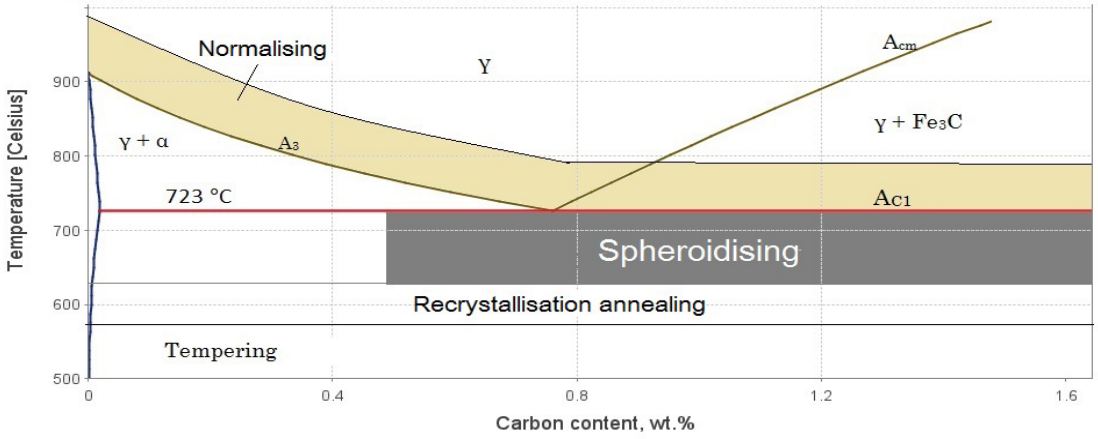

Fig. 2.3: Phase diagram of the iron-carbon system (up to 1.6 wt.% C) calculated using Thermo-Calc with fields indicating typical heat treatment temperatures re-drawn from ASM handbook [21].

As the pearlitic lamellar structure is never perfect in reality, there are always morphological growth faults that exist such as holes, kinks, striations, etc. Previous studies have shown that break-up of the lamellas during annealing happens within regions of such growth faults, that were generated during the initial formation of the pearlite. Spheroidisation can also initiate from these faults and expansion of such holes and thickening of the lamellas occurs [22], [23]. This continuous growth leads to break-up of large cementite platelets into small particles and then these small particles evolve into spheroids. The driving force is the chemical potential gradient between faults with various shapes and the neighbouring flat interfaces. In a 2D image the onset of spheroidisation appears as a coarsening in the lamellar thickness [23].

Moreover, with the addition of cold work, cementite lamellas break and step bands are created in some of the pearlite colonies in places where the lamellas break. Those places can become initiation points for spheroidisation. In case of hot deformation, preferential break-up sites are created by dislocation structures and are believed to accelerate spheroidisation by providing short circuit paths for diffusion. In addition, vacancies are being generated that increase diffusion rates of carbon and iron [3].

For temperatures far below the α-γ transformation line (A_{C1}), damage appears more slowly. Initially the pearlite lamellas start to break up and then coarsen until we get closer to A_{C1} where cementite lamellas turn into spheroids (Fig 2.4).

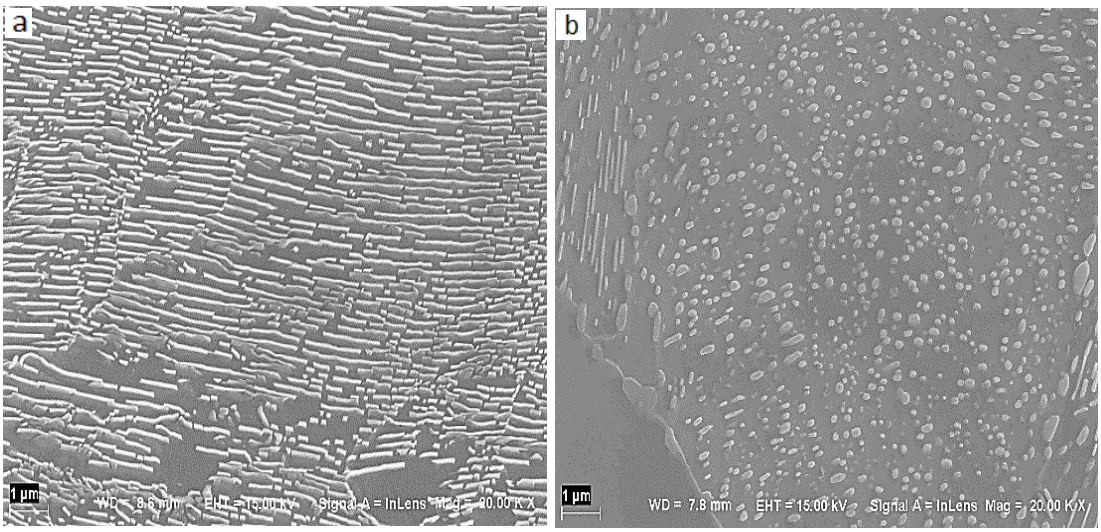

Fig. 2.4: Scanning electron micrographs of pearlite microstructure after heat treatment. (a) Initial lamella breakup, and (b) complete spheroidisation.

Given the above theoretical background, an attempt to connect this with railway wheel material was made in previous studies and in this thesis. First, exposure to high temperatures for longer times is known to cause softening of the material [9]. It was also found that longer time durations cause more pronounced spheroidisation [24]. Previous investigations combining low cycle fatigue loading and elevated temperatures have showed a cyclic hardening at 300 °C and cyclic softening at higher temperatures for virgin material ER7 [25],[26]. The change in room temperature (RT) hardness after exposure to elevated temperatures between 500 °C and 725 °C was also studied before for the ER8 grade [6]. It was also shown that the two grades ER7T and ER8T behave similarly under

cyclic loading with respect to hardening and softening, and only differ in stress levels due to the slight difference in carbon content.

2.2.4 Dislocation motion theory

Deformation in crystalline solids occurs with the generation, movement and accumulation of dislocations under an externally applied stress. Dislocation movement is limited by internal stress fields from different kinds of obstacles. The mobility of dislocations thus depend on thermally activated processes, such as cross-slip and climb, which enable dislocations to circumvent the obstacles [27]. The velocity with which they move depends on the rate they are able to overcome these obstacles [28]. For pure metals the main obstacles are stress fields from other dislocations but for alloys where atoms of different elements are in solid solution there are significant contributions from other sources as well [29]. The level of thermal activation that is necessary to overcome an obstacle is different depending on the kind of obstacle since these can have different strength or spacing between them [30]. Two regions exist for the dependence of the dislocation velocity with respect to stress and temperature. The first concerns low velocities and follows an Arrhenius-type behaviour, i.e. it increases with temperature, and the second concerns higher velocities where the temperature dependence is reversed. Only in the first region, dislocation motion is thermally activated [29], [31].

2.2.5 Strain ageing

Strain ageing in metals refers to the time-dependent phenomenon of impeding dislocation motion by segregation of mobile solute atoms. By diffusing to positions around dislocations where atoms find a low-energy position, and thus decrease the local stress level, these have the ability to temporarily arrest dislocations [32]. According to Cottrell-Bilby theory [33] it is a two-step process with the first step being the rearrangement of interstitials and formation of solute atmosphere around dislocations and the second being the formation of discrete clusters or precipitates [34]. In iron-based alloys and more specifically carbon steels this phenomenon is associated with interstitially dissolved atoms of carbon and nitrogen [35]. There are two types of strain ageing: static strain ageing and dynamic strain ageing.

Static strain ageing refers to the increase in yield stress and tensile strength that is observed in alloys when a specimen is strained to a certain level, then unloaded fully or partially and aged for a specific amount of time. After the ageing treatment, a higher stress response will be observed. Furthermore, in steels, static strain ageing causes the appearance of an upper and lower yield point and decreases the total elongation of the material [34].

In dynamic strain ageing (DSA), the dislocations are repeatedly pinned at obstacles during the straining process at high temperature, for example during a cyclic test at high temperature [36] or during a monotonic test. During such a test, dislocations surmount obstacles with the combined help of stress and thermal activation. Dislocation segments wait for a certain amount of time until they overcome the obstacle and then go to the next one with higher velocity. The diffusion of solute and interstitial atoms to the dislocations during this waiting time is called dynamic strain ageing or the Portevin-LeChatelier effect (PLC) [37]. This gives a serrated flow stress curve, seen after a tensile test with a suitable

combination of temperature and strain rate. DSA is responsible for the increased hardening that is observed during a cyclic fatigue test within a parameter window where strain rates and temperatures are producing this effect for the specific material and condition. So for both static and dynamic strain ageing the evolution of dislocation density has a great influence on the strain ageing process [36].

2.2.6 Dynamic strain ageing and low cycle fatigue tests

Fatigue life for a given stress amplitude and mean stress typically decreases with increasing temperature [38] (a few exceptions exist). When a material is subjected to a low cycle fatigue (LCF) experiment at elevated temperature and at low frequency, time-dependent processes such as creep, oxidation and dynamic strain ageing are influencing its mechanical behaviour (stress response including cyclic hardening) and fatigue life [39]. Except for this, dynamic strain ageing is shown during a LCF test as serrations, sudden load drops, jerkiness or other discontinuities in the stress-strain curve that give it the "staircase" type appearance. Serrated flow in cyclic tests can occur at lower temperatures than under monotonic deformation tests since non-equilibrium vacancies and dislocations that are generated during fatigue deformation enhance the diffusion of solute atoms. Another consequence of serrated flow is that it promotes localisation of plastic flow that in some cases leads to reduced fatigue life [40].

Dynamic strain ageing (DSA) is thus responsible for the increased hardening that is observed during a cyclic low cycle fatigue test within a parameter window where strain rates and temperatures are producing this effect for the specific material and condition. Both the hardening within one specific loop and the cyclic hardening (or softening) occurring throughout the fatigue life can be affected by DSA. So, apart from the serrated flow, the main effect of dynamic strain ageing during low cycle fatigue testing reported in the literature, is the increased cyclic hardening in a temperature range of 250–400 °C [35], [39].

2.2.7 Orientation gradients in pearlite

While interlamellar spacing, prior austenite grain size and other morphological features are important when evaluating the strength of pearlite and the sensitivity of the material to spheroidisation, there are other microstructural factors that can affect it, such as dislocation density or the amount of elements in solid solution.

Local misorientations in the microstructure are another factor that can affect the spheroidisation behaviour of the material. These are the result of a combination of the elastic strain field but more importantly they originate from the curvature of the crystal lattice that is associated with geometrically necessary dislocation density [41]. It was found that pearlitic ferrite (and presumably the cementite) contains orientation gradients (in contrast to the pro-eutectoid ferrite), which suggests that there is a certain density of geometrically necessary dislocations present [38]. It was concluded that in order to fully understand the mechanical properties of pearlite, the dislocation density of the pearlitic microstructure needs to be taken into account.

The heat-treated wheel material was evaluated using the EBSD technique to estimate dislocation density and distribution in a material as well as strain fields that exist in the material microstructure [43], [44].

3 Experimental procedures

3.1 Materials

The steels studied in the present work were the ER8 and the ER7 wheel steel grades. These materials follow the standard EN13262 [6] and their nominal compositions are shown in Table 3.1.

Table 3.1: Chemical composition of R8T and R7T wheel material, maximum levels, in wt.%

	C	***Si***	***Mn***	***Mo***	***Cr***	***Ni***	***S***	***P***	***V***	***Fe***
ER7 (R7T)	0.52	0.40	0.80	0.08	0.30	0.30	<0.015	0.020	<0.006	Bal
ER8 (R8T)	0.56	0.40	0.80	0.08	0.30	0.30	<0.015	0.020	<0.006	Bal

The rim chilling heat treatment (the wheel tread and flange are cooled with water jets after austenitisation) that these materials undergo during production creates a fine-pearlitic microstructure close to the rim with a slight decrease in hardness and strength and a slight increase in free ferrite and interlamellar spacing with increasing depth.

This investigation will cover the change in room temperature (RT) hardness after exposure to elevated temperatures of 250 to 650 °C for R8T grade material under the following conditions:

1. Undeformed (taken from an un-used wheel, “virgin material”)
2. After monotonic pre-straining to 6.5% plastic strain and
3. After cyclic pre-straining at $\Delta\varepsilon_t/2$=1.0% until saturation.

The degradation of the microstructure is registered and correlated to the hardness change measured. Material at larger depths below the wheel tread surface experiences slower cooling in production, which gives a decreasing hardness with depth. To extend the validity of the results to a wider range of heat treatments, or depth below the surface, hardness at increasing depth below the surface was measured and correlated with microstructural parameters examined by scanning electron microscopy and optical microscopy. Specifically, the ferrite content and lamellar spacing was measured at different depths for both undeformed R8T and R7T. Moreover, an attempt was made to complement the picture from the literature on mechanical behaviour at elevated temperature. This was accomplished by examining the low cycle fatigue (LCF) behaviour of the R7T material at elevated temperatures of 250 °C–600 °C and including hold times during which stress relaxation could be studied.

The last component of this study was to examine R8T wheel material using the EBSD technique for samples with different heat treatments and different pre-strain conditions.

3.2 Pre-straining

Tensile bars with 5 mm thickness and "dog bone" shape (see Fig. 3.1, dimensions in mm) were taken from a virgin R8T wheel at a depth of around 20 mm below the running surface. These bars were pre-strained using an Instron electro-mechanical tensile machine to 6.5% longitudinal strain. Two extensometers were used to prove an even strain distribution. Tests were run in strain control at a strain rate of 10^{-4} s^{-1}. Samples were taken from the waist of the pre-strained bars and cut into pieces around 5x8x8 mm, to be used for hardness testing and heat treatment experiments.

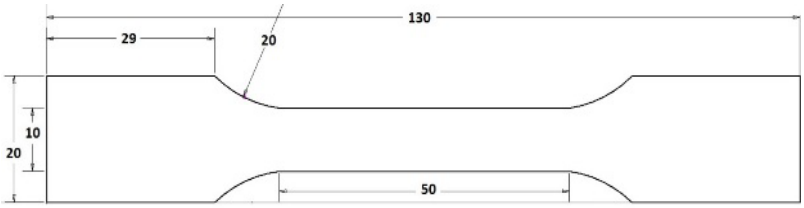

Fig. 3.1: Geometry of tensile test bars

Similar pieces were taken from cylindrical specimens from a depth of 15 mm below the running surface (Fig. 3.2) that had previously been exposed to uniaxial push-pull low cycle fatigue experiments at room temperature under constant strain amplitude loading at $\triangle\varepsilon_t/2$=1.0% run until failure (approximately 1300 cycles). All specimens were ground and polished down to 1 µm diamond suspension before the hardness measurements and heat treatments.

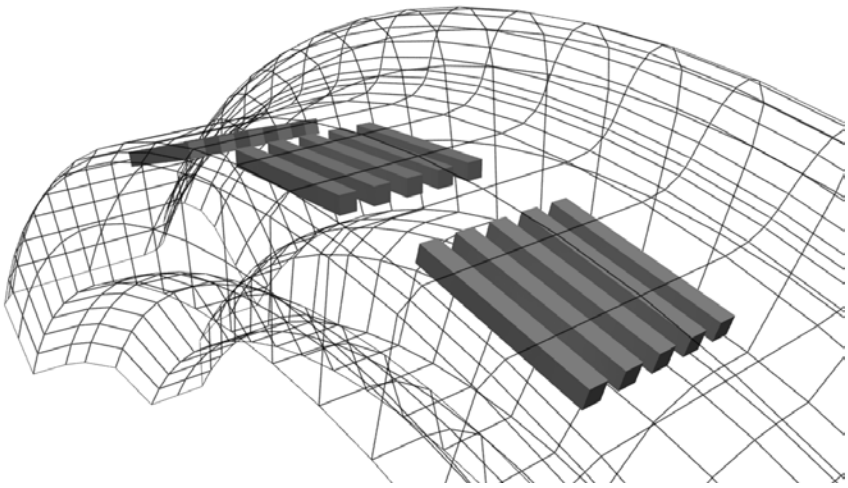

Fig. 3.2: Position of samples for LCF. All samples were extracted approximately at a depth of 15 mm below the wheel tread [45]

3.3 Heat treatments and hardness

Vickers hardness measurements were performed in undeformed and pre-strained conditions before heat treatment using an applied load of 10 kg in a Wolpert 2RC hardness

tester. Then the samples were put in a tube furnace with a nitrogen inert atmosphere to prevent oxidation and decarburisation. Both undeformed and pre-strained samples were heat treated for 4, 28 and 238 minutes at various temperatures in the range 250–650 °C. After heat treatments at selected times and temperatures, new room temperature hardness measurements were performed, again with a 10 kg load. For both measurement series, indentations were placed randomly on the specimen surface at a distance more than twice the diagonal length from the previous indentation. The hardness was taken as the mean value of three indentations that were measured with an optical microscope afterwards to decrease the error in reading.

3.4 Mechanical testing

These tests were performed on virgin wheels of the R7T material and samples were taken from the wheel rims parallel to the running direction at a depth of approximately 15–20 mm below the running surface. Cylindrical tensile test bars with gauge diameter 6 mm were produced and ground to 800 grit. Low cycle fatigue tests were run in an Instron servo-hydraulic test frame in strain amplitude control mode. Tests were run at constant total strain amplitude $\Delta\varepsilon_t/2$ of 0.6% with triangular wave shape at $R\varepsilon=-1$ and strain rate 5×10^{-3} s^{-1} giving a cycle time of 4.8 s. (Tests with $\Delta\varepsilon_t/2$ = 0.4% and $\Delta\varepsilon_t/2$ = 1.0% were also run under the same conditions, but these are not addressed in this thesis). Peak/trough values were recorded for every cycle, and full hysteresis loops were recorded for the initial 25 cycles and thereafter regularly during their lifetime. Several tests were run with hold periods repeating every 500 cycles. These hold periods had a duration of 30 min, and the stress relaxation under constant compressive strain of -0.6% was recorded. The test durations varied between 4 and 8 h depending on temperature. The machine was equipped with a furnace to perform isothermal tests at elevated temperatures from 250 °C to 600 °C without atmosphere control. Specimens were first mounted in the grips, then the furnace was sealed with insulation wool and heated until the temperature of the specimen became stable at the desired level. All tests were run under constant temperature until failure.

3.5 Microstructure investigation

Light optical microscopy (OM) and scanning electron microscopy (SEM) were used to evaluate the initial and final microstructures. In addition, the electron backscatter diffraction (EBSD) technique was employed to evaluate the orientation gradients of the material in its initial and as-heat-treated condition. The specimens were mechanically ground and polished to 0.04 µm using a colloidal silica suspension. Etching was done using Nital (3% HNO_3 in ethanol) to gain some topographical contrast and thus be able to map regions of interest. The high-resolution micrographs and the EBSD measurements were carried out in a LEO 1550 high-resolution field emission scanning electron microscope (FEG-SEM). The system was equipped with an EBSD detector (Nordlys, Oxford instruments), a high-speed camera for EBSD pattern recording and software for crystal orientation mapping (AZtecHKL). The samples were tilted to have their normal at 70° to the incident beam and the SEM was operating at an accelerating voltage of 20 kV. Crystallographic orientation maps were taken on the pearlite colonies as well as on the pro-eutectoid ferrite with a step size of 130 nm, which is around the interlamellar spacing of the pearlite in this material. The EBSD patterns of the pearlitic cementite were of insufficient quality and were thus omitted from the analysis. For the grain boundary

maps, low angle boundaries (LAB) were selected between 2° and 10° (marked with red lines) and high angle boundaries (HAB) higher than 10° (marked with black lines).

Another useful map type for this investigation is the kernel average misorientation map (KAM). This type of map reveals short-range orientation gradients and allows us to distinguish between local orientation changes and sub-boundaries. For this calculation, the average misorientation between a point on the measurement grid and its neighbours is measured. Misorientations between all neighbouring points within the kernel are then averaged, and to exclude the grain boundary effect a 3° cut-off angle was used as a filter to only focus on small rotations that could also indicate a high dislocation density. For this study, a square scanning grid was used as shown in Fig. 3.3, and from that, the 2nd neighbour shell (5x5) was used to evaluate the material.

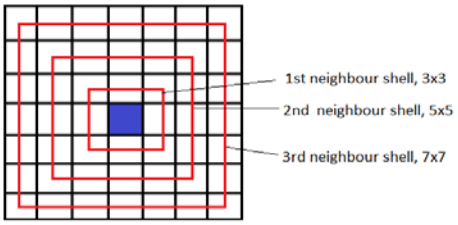

Fig. 3.3 Kernel shells for a square grid

In order to determine the pearlite interlamellar spacing, a series of circular test grids with constant diameter (5 μm) was randomly superimposed on pearlite colonies imaged at a constant magnification. The number of interceptions was counted and the mean random spacing (δ_r) was calculated as:

$$\delta_r = \frac{\pi d_c}{n} \tag{2}$$

where d_c is diameter of circular grids and n is the number of interceptions. This method ensures a more randomised and unbiased measure of interlamellar spacing [46]. The data was later converted to the mean directed spacing for each circular test grid. In order to determine the true lamellar spacing, the influence of sectioning angle was compensated for. This was performed by generation of the cumulative probability of true lamellar spacing based on observed apparent spacing. In the final step, the distribution of true lamellar spacing was estimated by inverse identification of parameters (μ and σ) of the normal distribution probability function (see Equation 3), giving the least deviation between the experimental and estimated cumulative probabilities.

$$P(L) = \frac{1}{\sigma\sqrt{2\pi}}\, e^{\frac{-(L-\mu)^2}{2\sigma^2}} \tag{3}$$

where μ and σ represent mean value and standard deviation. The key advantage of this method is to obtain the distribution of true lamellar spacing, in addition to the value of

mean true lamellar spacing, frequently reported in literature as the only parameter to characterise pearlitic steels.

In addition, depth profiles were acquired for the two materials in the undeformed state and the microstructure was characterised to evaluate the gradual changes developing during the rim chilling process in production. The free ferrite content of undeformed R8T and R7T was measured using the optical microscope and the phase identification module of the Axio Visio software.

4 Results and summary of appended papers

This section presents a selection of the main results and analysis, for the performed experiments.

4.1 Hardness measurements

The effect of the heat treatments is shown in Fig. 4.1. The initial hardness value for the virgin material, also called "undeformed" R8T, is around 260 HV10 (Fig. 4.1a), around 274 HV10 for the monotonically strained condition (Fig. 4.1b) and around 309 HV10 for the cyclically strained R8T (Fig. 4.1c).

From Fig. 4.1a-b, it is clear that a hardening process is taking place at around 300 °C for the undeformed and the monotonically strained materials, whereas for the cyclically strained material (Fig. 4.1c) this is less obvious. The main reason for this hardening is strain ageing. When the material is monotonically strained and then annealed, static strain ageing gives a higher work hardening effect than seen for the undeformed condition. For the cyclically strained material, dislocations that were generated during the testing are annealed from the heat treatment which counteracts the effect of static strain ageing and thus this condition shows a lower work hardening effect.

The hardening seems to be more pronounced when the material is subjected to 28 min heat treatments, in the case of both the virgin and the monotonically strained material. At temperatures above 350 °C, softening occurs for all three time durations. For the temperature range 400–450 °C, both of the above conditions have lost a few percent in hardness, whereas the cyclically strained material undergoes severe softening in this temperature range. After 500°C, severe softening for all conditions is observed.

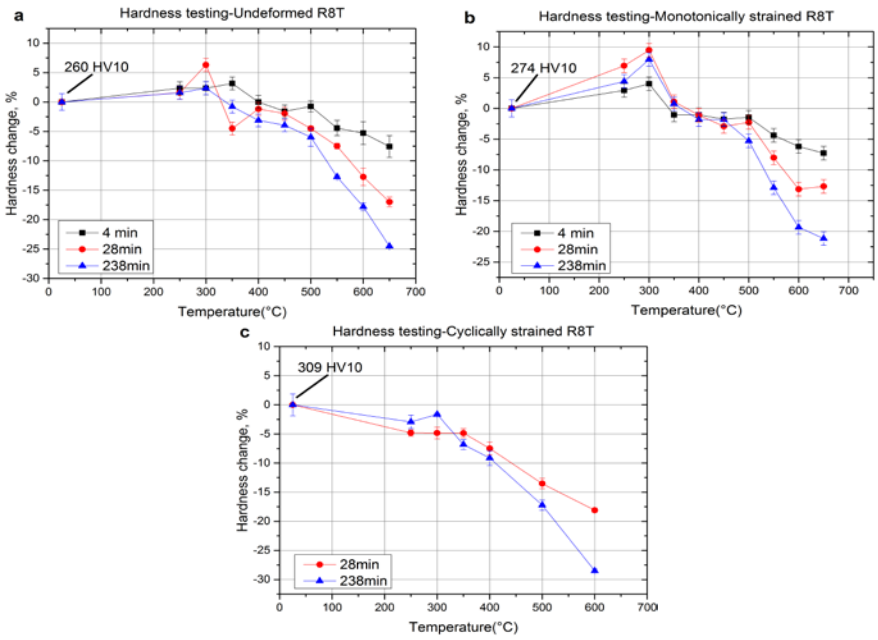

Fig. 4.1: Hardness change after heat treatments of R8T material for (a) undeformed (b) monotonically strained and (c) cyclically strained

It can be concluded from the above observations that exposure to high temperatures has a large influence on the hardness of the material. The above results indicate that plastic

deformation combined with exposure to high temperatures, for example after excessive braking in train operation, will have a great impact on the mechanical properties of the material.

4.2 Low Cycle Fatigue Behaviour

To complement the above hardness measurements with behaviour at elevated temperatures, low cycle fatigue tests on R7T were performed. These experiments showed again the strong influence of temperature on the peak stress development, see Fig. 4.2 (the equivalent graph with the trough stress development during the compressive segments of the test shows very similar results with the lines mirrored towards the negative values).

At 300 °C, there is a strong initial hardening that decreases to slight hardening during the remainder of the fatigue life (seen in the range 10–80% of the fatigue life, thereafter major cracks influence the stresses registered). At 250 °C, the hardening is even stronger than at 300 °C and it appears later in the fatigue life. The mechanism behind this hardening is dynamic strain ageing, with locking of dislocations by interstitials [39]. At 350 °C, thermal softening, i.e. increased mobility of dislocation following increased thermal activation sets in, and at 400 °C, this mechanism dominates, giving lower peak stresses with time as compared to the room temperature behaviour seen in Fig. 4.2 (left). At the two higher temperatures, 500 °C and 600 °C, the material exhibits considerably lower peak stresses and cyclically softens during the fatigue life as a result of combined thermal softening and microstructural degradation.

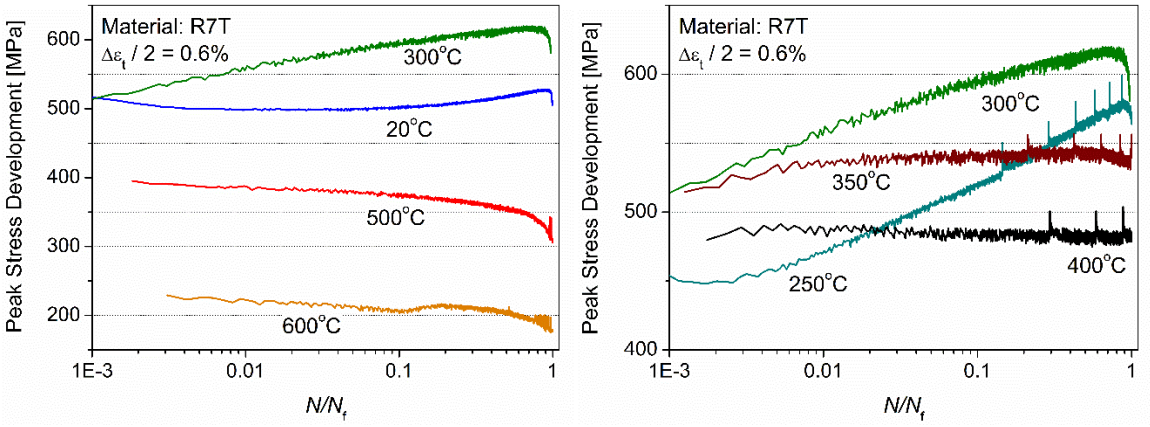

Fig. 4.2: Peak stress development in the interval 250–600 °C with a room temperature curve also reported for reference.

It is clear from these results that similar behaviour is observed around 300 °C for both R7T and R8T with pronounced hardening occurring and severe softening for higher temperatures.

4.3 Microstructure

These two steels have a similar composition with only a slight difference in carbon content. Hence, their microstructure looks almost identical. The initial microstructure

consists of pearlite (dark areas in Fig. 4.3a, b) and some pro-eutectoid ferrite (appearing bright in Fig. 4.3a, b).

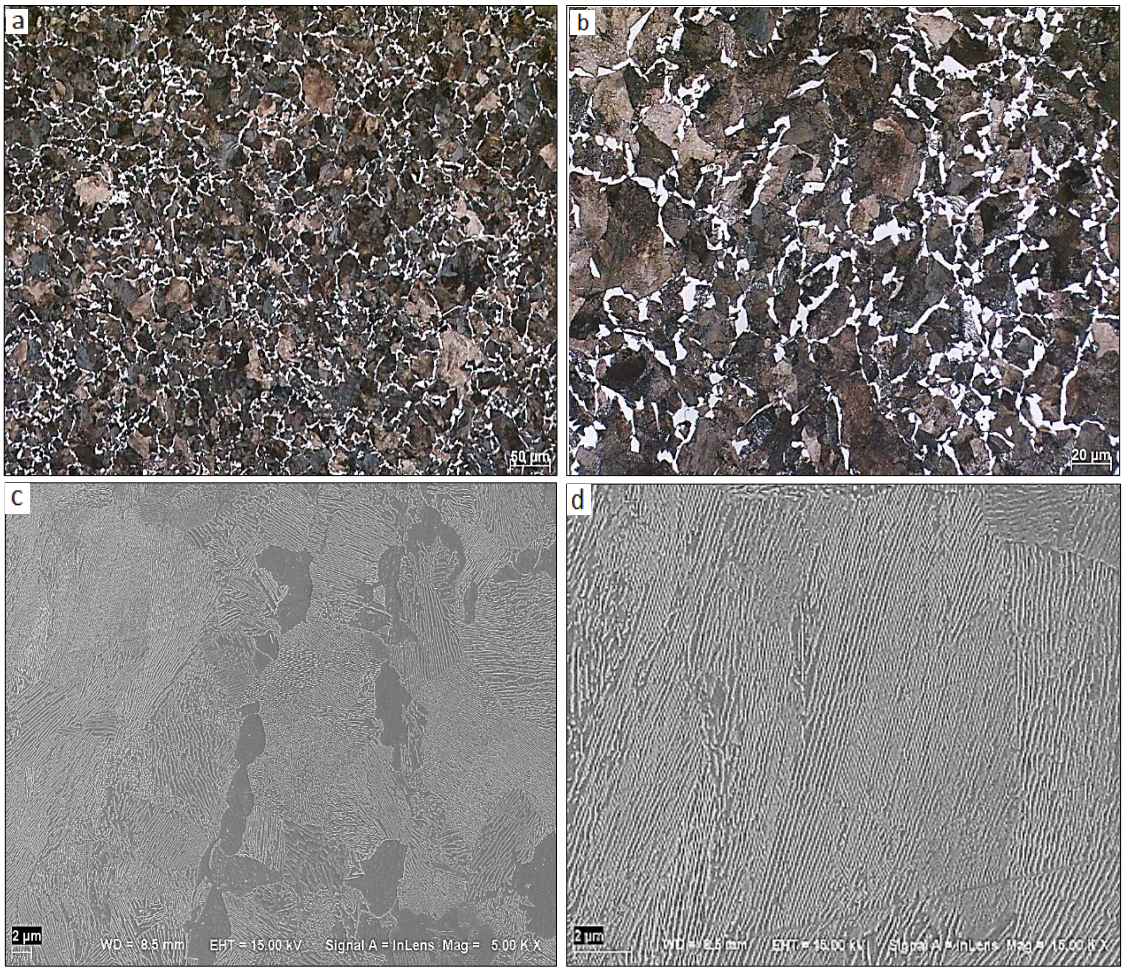

Fig. 4.3: Microstructural overview of the undeformed R8T using optical microscopy (a, b) and SEM (c, d) at different magnifications.

The interlamellar spacing was calculated at three different depths using SEM micrographs (Fig. 4.3c, d). The mean true interlamellar spacing values along with the standard deviations appear on table 4.1.

Table 4.1: Mean true interlamellar spacing (nm)

Depth (mm)	*R8T*	*St. deviation*	*R7T*	*St. deviation*
20	132	5.6	125	8.7
40	145	9.5	134	4.1
60	157	8.7	146	12.8

It is clear that the spacing is finer close to the surface and gets coarser as we move further down from the surface of the wheel. One would expect the R8T with the higher carbon content to have finer spacing [16] but cooling rates could have a stronger effect.

The ferrite content is shown in Fig. 4.4. It increases from 8.2 at 20 mm depth up to 12.2 vol.% at 60 mm depth for R8T and correspondingly from 11.3 to 14.4 vol.% for R7T.

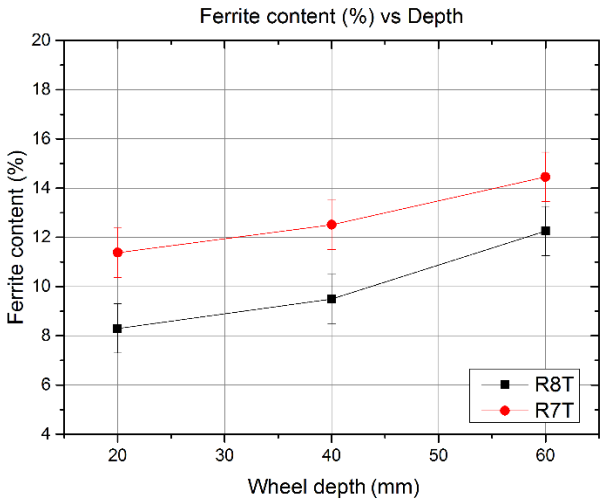

Fig. 4.4: Ferrite content with increasing depth

Table 4.2 shows the hardness measurements at the three depths. It is clear that the material softens with increasing depth since the free ferrite content increases and the interlamellar spacing increases. R8T has slightly higher hardness than R7T as expected. An unexpectedly high hardness value for R7T at 60 mm depth was measured, but is thought to be due to measurement inaccuracy and sampling, combined with a larger standard deviation in the R7T interlamellar spacing at 60 mm depth.

Table 4.2: Hardness with increasing depth

Depth(mm)	***Hardness (HV10)***	
	R8T	*R7T*
20	268	266
40	254	252
60	242	253

The SEM investigation of the undeformed material, after the annealing treatments, showed that the pearlite lamellas start to break up at around 450 °C (Fig. 4.5) with a more pronounced effect for longer durations. This could also explain the small drop in hardness as seen in Fig. 4.1a. The same degree of spheroidisation happens earlier for the

monotonically strained material at around 400 °C. It appears that pre-deformation of the material has an effect on the microstructure degradation.

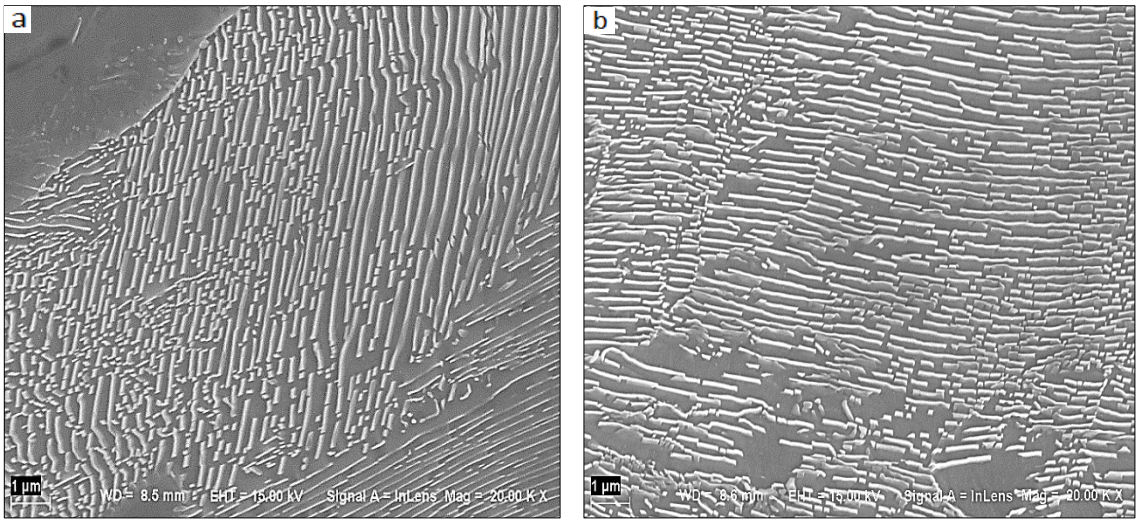

Fig. 4.5: SEM micrographs of the R8T material heat-treated for 238 min a) undeformed at 450 °C and b) monotonically strained at 400 °C

Higher temperatures and longer times allow for stronger spheroidisation, which correlates to the increasing drop in hardness. It is shown in Fig. 4.6 that severe spheroidisation is taking place for temperatures over 500 °C. Similar results were obtained for the cyclically strained R8T material.

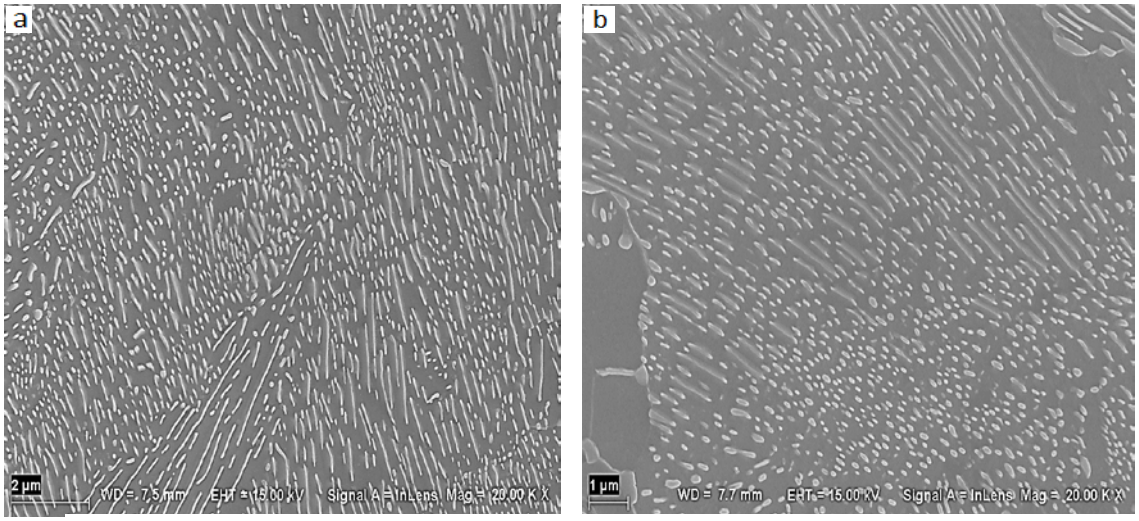

Fig. 4.6: SEM micrographs of the monotonically strained R8T heat-treated for 238 min at a) 500°C and b) 600°C

It is obvious from these micrographs that the combined influence of plastic deformation and thermal exposure causes degradation of the microstructure. First, the lamellas break up due to the deformation and the heat treatment, and then through further coarsening spheroidisation of the cementite particles occurs. This in turn causes the decrease in room temperature hardness that is observed, which is more severe for longer durations and higher temperatures.

4.4 EBSD analysis

This section includes the latest results and some preliminary conclusions of an ongoing investigation, and as such, they only partly appear in the second paper. Wheel material R8T was examined in this EBSD analysis. As a reference point, an undeformed specimen was examined to evaluate the initial state of the material microstructure after production. A random area was selected without taking into account any specific pearlite colony or other microstructural features. The grain boundaries map along with the kernel average misorientation map is shown in Fig 4.7. One can observe from these that many sub-grain boundaries exist (showing as red lines on grain boundary maps) along with a strong local misorientation, which suggests that a high dislocation density is present in the initial microstructure that is contributing to the material's initial mechanical properties.

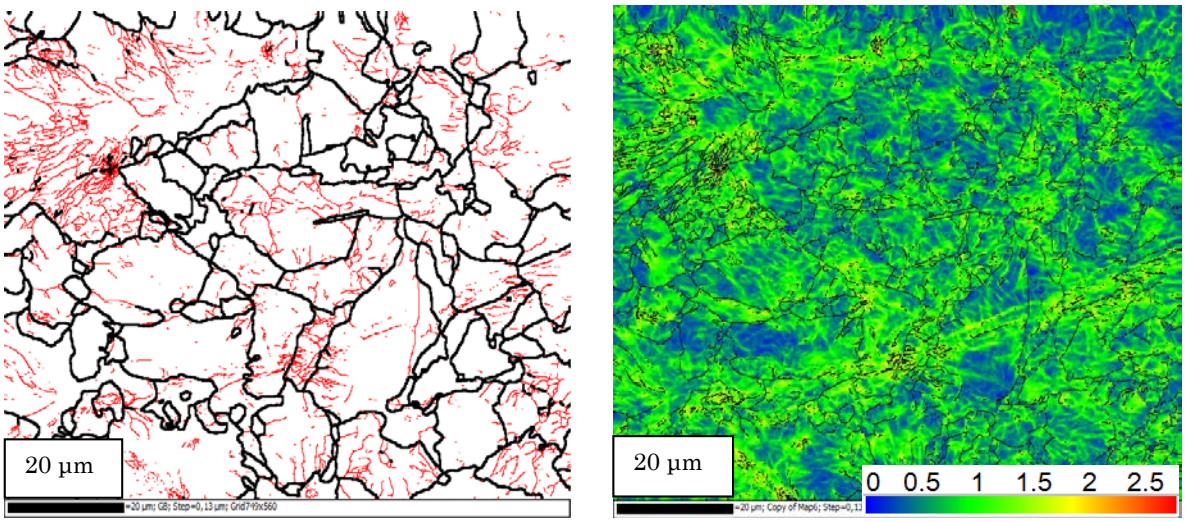

Fig. 4.7: Microstructural mapping of undeformed R8T material at room temperature using the grain boundary plot with red lines for LAB between 2-10° and black lines for HAB >10° (left) and Kernel average misorientation map (right) using orientations up to 2nd neighbour shell.

In Fig. 4.8, an SEM micrograph along with the inverse pole figure map is shown for R8T after annealing at 300 °C.

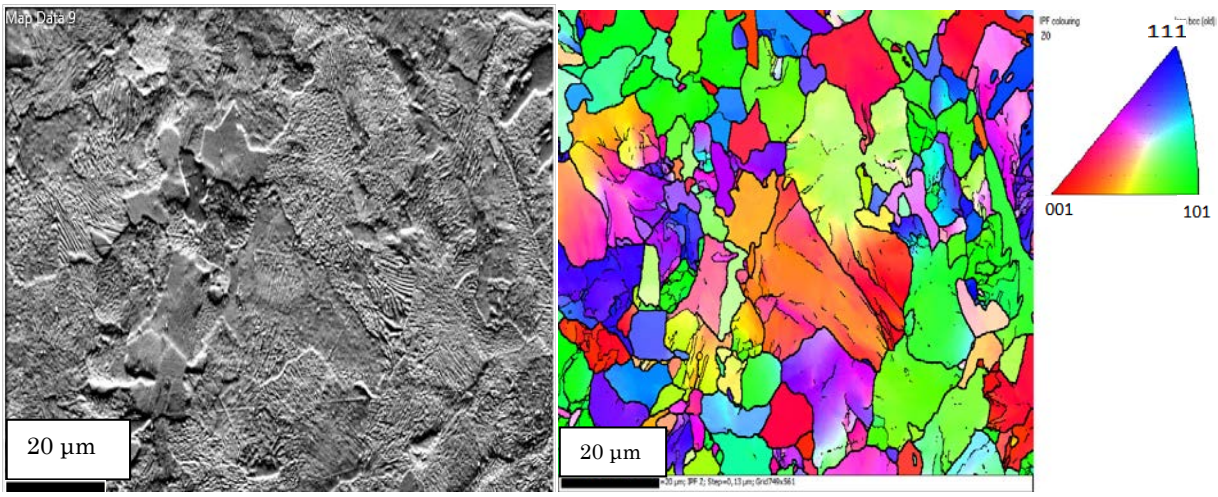

Fig. 4.8: Microstructure of undeformed R8T material after annealing at 300°C using the forescatter detector (left) and texture mapping using the inverse pole figure (IPF) colour code of the crystallographic normal vector (right)

Pearlite colonies appear to have orientation gradients as reported in the literature while pro-eutectoid ferrite grains are shown with a single colour and thus a single orientation. The grain boundaries and KAM for this condition are show on Fig. 4.9. No apparent microstructural degradation is taking place at this temperature but it is clear that dislocation density has dropped significantly after annealing. Ferrite grains that appear mostly blue in the KAM plot seem to have no sub-grain boundaries and most of these low-angle boundaries are concentrated in the pearlitic colonies.

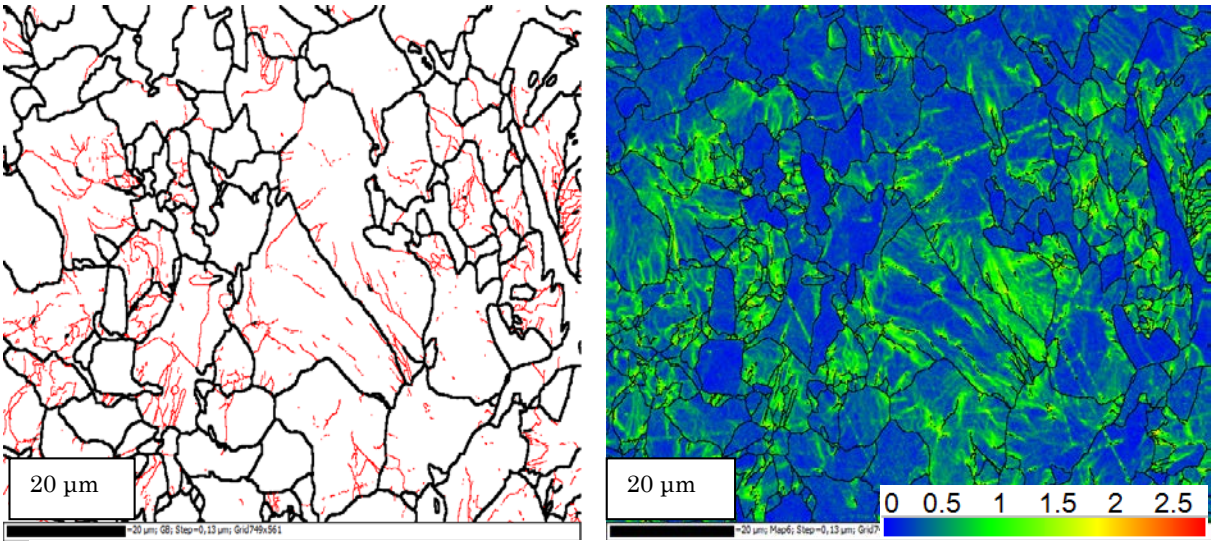

Fig. 4.9: Microstructural mapping of undeformed R8T material after annealing at 300°C using the grain boundary plot with red lines for LAB between 2-10° and black lines for HAB >10° (left) and Kernel average misorientation map (right) using orientations up to 2nd neighbour shell.

When annealing at even higher temperatures (at 500°C) spheroidisation starts to occur. In Fig 4.10, a micrograph of this temperature is shown with an IPF map. Spheroidised colonies appear to start losing the previous orientation gradients seen in the pre-existing pearlite colonies (c.f. Fig. 4.8, right).

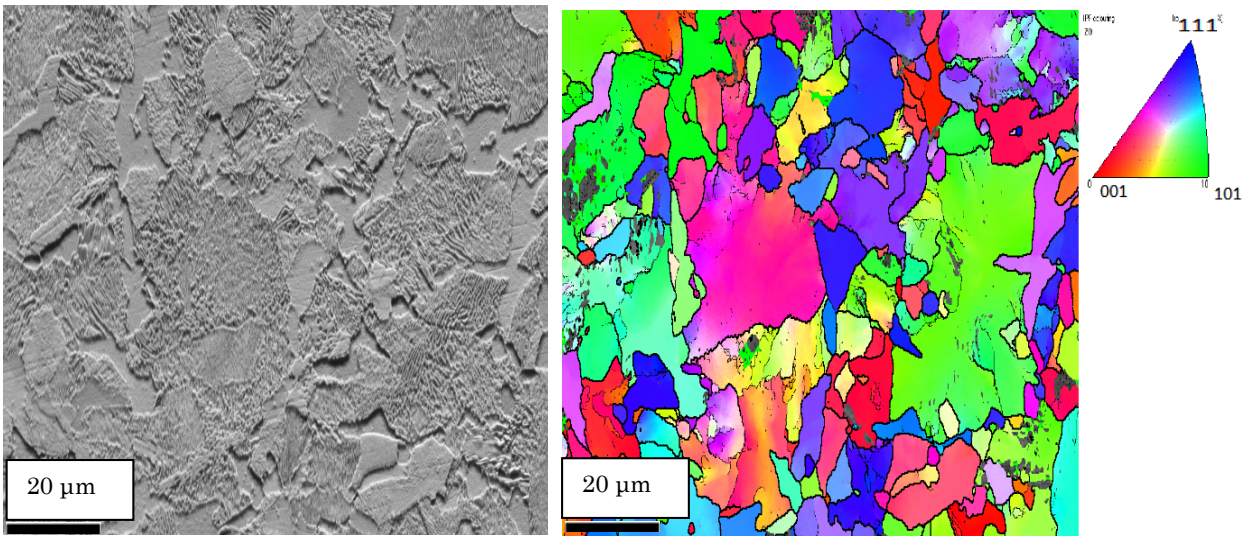

Fig. 4.10: Microstructure of undeformed R8T material after annealing at 500°C (left) and texture mapping using the inverse pole figure (IPF) colour code of the crystallographic normal vector (right)

The same investigation was also performed for the monotonically strained R8T. A comparison of the grain boundary and KAM maps between the two conditions for various temperatures is shown in Fig. 4.11 and 4.12 that will allow for some better overview and comparison. All the samples appearing in Fig. 4.11 and 4.12 were heat-treated for 4 hours. The monotonically strained material seems to have a higher number of sub-grain boundaries that seem not to anneal as fast as the undeformed material even at the higher temperatures.

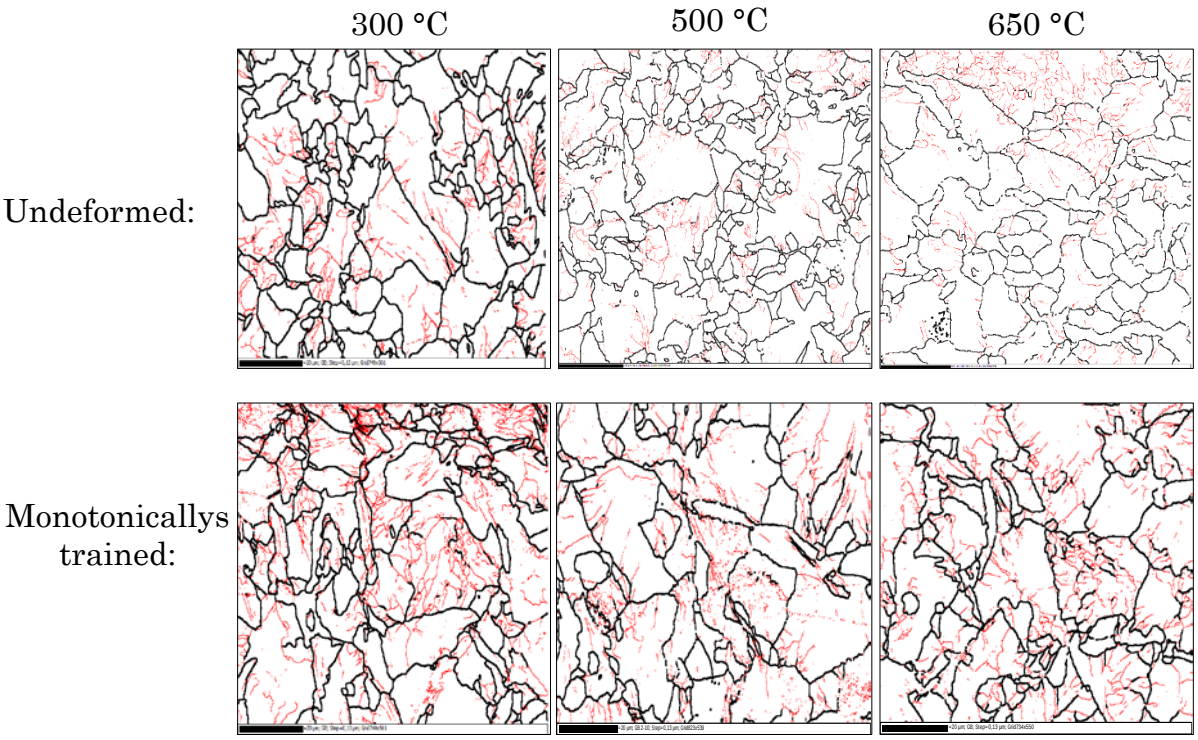

Fig. 4.11: Grain boundary maps comparison between undeformed and monotonically strained R8T at various temperatures (red lines for LAB between 2-10° and black lines for HAB >10°), scaling as in Fig. 4.7, 4.9

Ferrite grains appear with no local misorientation (blue colour) in the undeformed material KAM maps whereas in the monotonically strained ones they seem to have some degree of misorientation and a larger part of the field of view is showing as green. One possibility is that since pre-straining makes the material more prone to spheroidisation as shown previously from the heat treatments, cementite carbon might be diffusing from previous pearlite colonies to the pro-eutectoid ferrite grains and precipitating there. Given that this isstill under evaluation further analysis of the results will be performed in the near future.

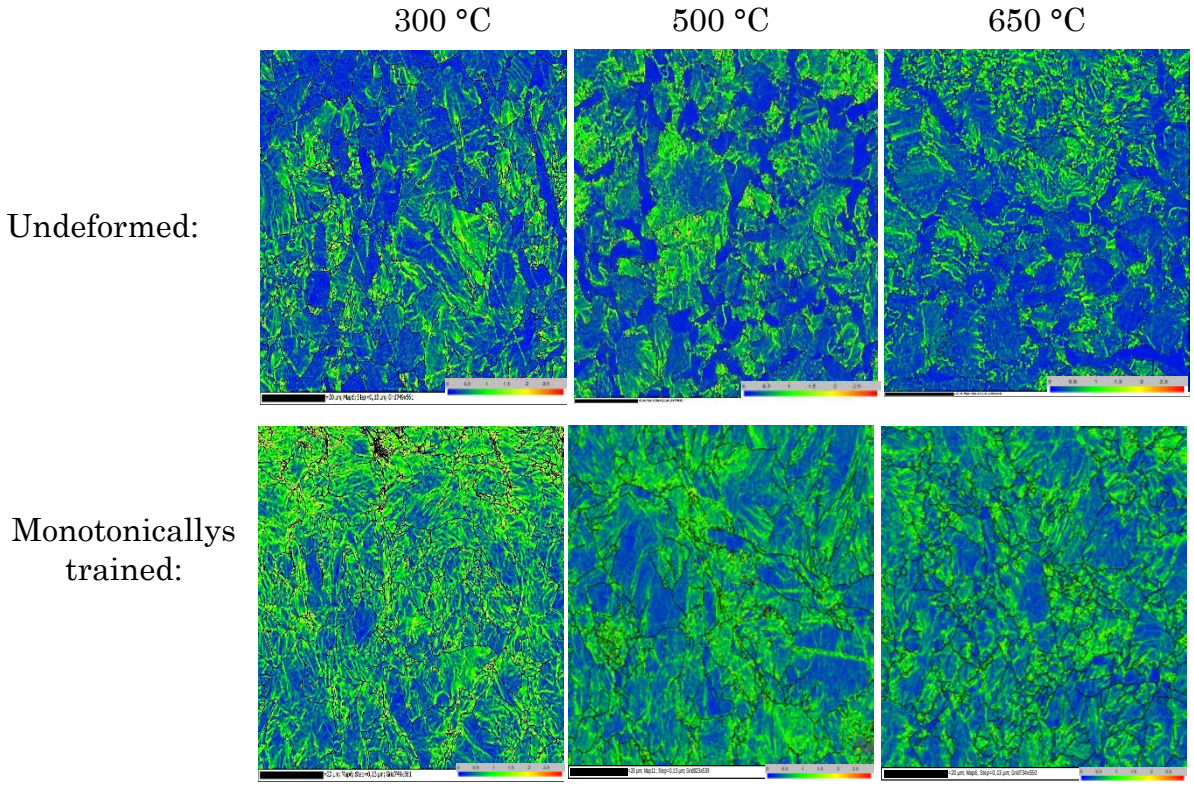

Fig. 4.12: Kernel average misorientation maps comparison between undeformed and monotonically strained R8T at various temperatures, colour scale and scaling as in Fig.4.7, 4.9

4.5 Final remarks and conclusion

The effect of combined thermal and mechanical loadings on the mechanical behaviour of near-pearlitic railway wheel steels was evaluated. The two materials R8T and R7T exhibit a slight difference in carbon content and may show a slight difference in hardness but otherwise behave similarly. The hardness tests performed at room temperature isolate the effect of microstructural degradation, while the elevated temperature low cycle fatigue tests show the combined influence of microstructural degeneration and thermal softening due to increased thermal activation at higher temperatures.

Annealing treatments of R8T and evaluation of cyclic mechanical properties of R7T allowed for the following conclusions.

- The room temperature hardness increase after annealing at around 300 °C is evident for both un-deformed and monotonically strained conditions. It is more pronounced in the monotonically strained material despite the higher starting level. After annealing above 350°C room temperature hardness does not change much, until 450 °C for the monotonically strained, and 500 °C for the un-deformed material. Decrease in hardness at 500 °C was around 5% for both conditions, and reached almost 22% at 650 °C for the monotonically strained material. The cyclically strained material softens at all temperatures, and reaches a 30% decrease already after annealing at 600 °C.

- Hardening was also observed during the low cycle fatigue tests performed at around 300 °C due to dynamic strain ageing. Cyclic hardening starts rather strongly in the beginning of the fatigue life and then continues at a decreasing rate. At 500 °C, cyclic softening can be observed during the entire fatigue life. Hold times showed that the material exhibits stress relaxation due to viscous effects from temperatures at around 250–300 °C, increasing strongly with temperature. The influence of hold times on the stress-strain loop during further cycling is small.

- After heat treatments, the microstructure evaluations showed that pearlite lamellas in the un-deformed material start to break up at around 450 °C, with a more pronounced effect for longer heat treatment durations and higher temperatures. Pearlite lamellas begin to break up earlier for both pre-strained states at around 400 °C. Some regions remain seemingly unaffected by temperature, and deformation localised to certain colonies and free ferrite could be a possible explanation.

Interlamellar spacing as well as free ferrite have been characterised and found to increase with increasing depth below the running surface of the wheel for both materials studied. As a result of the above, hardness values decrease gradually with increasing depth below the running surface. During the life cycle of a wheel, maintenance such as re-profiling by wheel turning is performed at regular intervals. This means that the hardness of the new surface will be slightly lower than the initial state due to the hardness gradient. However, during run-in, the surface will experience work hardening and residual stresses will develop, increasing the strength of the surface layer. Based on the observations above and the literature on near-pearlitic steels, it is believed that the results and conclusions drawn above are valid not only for the virgin surface region, but throughout the depth of the wheel tread exposed to mechanical and thermal loads during the wheel's service life.

From the EBSD analysis so far, it can be seen that:

- Large pearlite colonies appear to have orientation gradients due to the initial formation of the pearlite, while ferrite grains have a more uniform orientation.

- Spheroidised pearlite colonies appear to have lost their initial orientation gradients and obtain a more uniform orientation after spheroidisation. These mostly contain low-angle boundaries.

- Large initial orientation gradients are present in the material in its undeformed state that is reduced with increasing temperature (drops already at 300°C) but orientation gradients remain rather stable for monotonically strained R8T.

5 Future work

Finalising the EBSD analysis is the next part of the project, along with an attempt to examine and quantify the amount of spheroidisation that takes place at various temperatures and different pre-strained conditions. This will help to correlate microstructure with the mechanical properties of the material. Different approaches for quantification will be examined with the aim of creating a software tool that can use SEM micrographs and provide as output the percentage of spheroidised lamellas for a given sample.

The project will then shift focus, and also include rail material. Bi-axial testing (tension-compression and torsion) of rail material R260 will begin, first at room temperature and eventually move to high-temperature testing. A possible future expansion is to characterise the thermo-mechanical fatigue (TMF) properties, i.e. a varying temperature during the mechanical cyclic deformation.

6 Acknowledgments

First and foremost, I would like to express my appreciation and gratitude to my supervisor Docent Johan Ahlström, who has given me guidance and support throughout the project.

The contribution and input of the reference group members to this project is greatly appreciated.

I would also like to thank and acknowledge Amir Malakizadi for the contribution in the first paper and numerous discussions about pearlite☺. Also all colleagues and friends in the Department of Materials and Manufacturing Technology and the Department of Applied Mechanics are gratefully appreciated for their kindness, support and for making every working day a little bit special.

Finally I would like to thank my fiancé Evangelia Varagka, who had to move here in Sweden because of me, for all the patience and understanding during this period. Lastly a big thank you goes to my family back in Greece for all their support.

7 References

[1] R. Lundén and B. Paulsson, *Introduction to wheel—rail interface research*. Woodhead Publishing Limited, 2009.

[2] F. Walther and D. Eifler, "Fatigue behaviour of railway wheels at different temperatures," *Mater. Test.*, vol. 46, no. Lm, pp. 158–162, 2004.

[3] S. Chattopadhyay and C. Sellars, "Kinetics of pearlite spheroidisation during static annealing and during hot deformation," *Acta Metall.*, vol. 30, pp. 157–170, 1982.

[4] J. Ahlström and B. Karlsson, "Microstructural evaluation and interpretation of the mechanically and thermally affected zone under railway wheel flats," *Wear*, vol. 232, pp. 1–14, 1999.

[5] J. Ahlström and B. Karlsson, "Analytical 1D model for analysis of the thermally affected zone formed during railway wheel skid," *Wear*, vol. 232, no. 1, pp. 15–24, 1999.

[6] N. F. En, "European standard for Wheels —EN 12262- Product requirements," 2009.

[7] Y. Okagata, "Design Technologies for Railway Wheels and Future Prospects," *Nippon STEEL SUMITOMO Met. Tech. Rep. No. 105*, no. 105, 2013.

[8] K. Mädler and M. Bannasch, "Materials used for Wheels on Rolling Stock," *7th World Congr. Railw. Res.*, 2006.

[9] K. Cvetkovski, J. Ahlström, and B. Karlsson, "Thermal degradation of pearlitic steels: influence on mechanical properties including fatigue behaviour," *Mater. Sci. Technol.*, vol. 27, no. 3, pp. 648–654, 2011.

[10] D. A. Porter, K. E. Easterling, and Y. Sherif, *Phase Transformations in Metals and Alloys*, vol. 3, no. 1. 2009.

[11] H. K. D. H. Bhadeshia and R. W. K. Honeycombe, *Steels--Microstructure and Properties*. 2006.

[12] A. R. Marder and B. L. Bramfitt, "The Effect of Morphology on the Strength of Pearlite," *Proc. Int. Conf. Strength Met. Alloy.*, vol. 7, no. March, pp. 822–823, 1970.

[13] N. Guo and Q. Liu, "Back-scattered electron imaging combined with EBSD technique for characterization of pearlitic steels," *J. Microsc.*, vol. 246, no. 3, pp. 221–228, 2012.

[14] O. P. Modi, N. Deshmukh, D. P. Mondal, A. K. Jha, A. H. Yegneswaran, and H. K. Khaira, "Effect of interlamellar spacing on the mechanical properties of 0 . 65 % C steel," *Mater. Charact.*, vol. 46, pp. 347–352, 2001.

[15] J. Hyzak and I. Bernstein, "The role of microstructure on the strength and

toughness of fully pearlitic steels," *Metall. Trans. A*, vol. 7, no. August, 1976.

[16] C. M. Bae, C. S. Lee, and W. J. Nam, "Effect of carbon content on mechanical properties of fully pearlitic steels," *Mater. Sci. Technol.*, vol. 18, no. 11, pp. 1317–1321, 2002.

[17] K. K. Ray and D. Mondal, "Effect of interlamellar spacing on strength of pearlite in annealed eutectoid and hypoeutectoid plain carbon steels," *Acta Metall. Mater.*, vol. 39, no. 10, pp. 2201–2208, 1991.

[18] S. Suresh, "Fatigue of materials," *Materials & Design*. p. 679, 1998.

[19] L. E. Miller and G. C. Smith, "Tensile Fractures in carbon steels," *J Iron Steel Inst (London)*, vol. 208, no. pt 11. pp. 998–1005, 1970.

[20] M. Dollar, I. M. Bernstein, and A. W. Thompson, "Influence of deformation substructure on flow and fracture of fully pearlitic steel," *Acta Metall.*, vol. 36, no. 2, pp. 311–320, 1988.

[21] T. B. Massalski, *Binary Alloy Phase Diagrams*, vol. 2. 1990.

[22] M. X. Zhang and P. M. Kelly, "The morphology and formation mechanism of pearlite in steels," *Mater. Charact.*, vol. 60, no. 6, pp. 545–554, 2009.

[23] Y. L. Tian and R. W. Kraft, "Mechanisms of Pearlite Spheroidization," *Metall. Trans. A*, vol. 18, no. August, pp. 1403–1414, 1987.

[24] D. Nikas and J. Ahlström, "Thermal deterioration of railway wheel steels," in *36th Riso international symposium of material science*, 2013.

[25] C. J. Peters and D. Eifler, "Influence of Service Temperatures on the Fatigue Behaviour of Railway Wheel and Tyre Steels," *Mater. Test.*, vol. 51, no. 11–12, pp. 748–754, Nov. 2009.

[26] J. Ahlström, "LCF Loop shape in near pearlitic steels - Influence of temperature," in *Proceedings of 7th International Conference on Low Cycle Fatigue, Aachen*, 2013.

[27] B. Wielke, "Thermally activated dislocation movement at plastic deformation," *Czechoslov. J. Phys. B*, vol. 31, no. 2, pp. 142–156, 1981.

[28] G. Schoeck, "The Activation Energy of Dislocation Movement," *Phys. Status Solidi*, vol. 8, no. 2, pp. 499–507, 1965.

[29] P. S. Follansbee and U. F. Kocks, "A constitutive description of copper based on the use of the mechanical threshold stress as an internal state variable," *Acta Mater.*, vol. 36, no. 1, pp. 81–93, 1998.

[30] G. Schoeck, "The superposition of thermal activation in dislocation movement," *Phys. Status Solidi*, vol. 87, no. 2, pp. 571–581, 1985.

[31] M. Hiratani and E. M. Nadgorny, “Combined Modelling of Dislocation Motion with thermally activated and Drag-Dependent Stages,” *Acta Met.*, vol. 49, pp. 4337–4346, 2001.

[32] S. D. Mesarovic, “Dynamic strain aging and plastic instabilities,” *J. Mech. Phys. Solids*, vol. 43, no. 5, pp. 671–700, 1995.

[33] A. H. Cottrell and B. A. Bilby, “Dislocation Theory of Yielding and Strain Ageing of Iron,” *Proc. Phys. Soc. Sect. A*, vol. 62, no. 1, pp. 49–62, 2002.

[34] M. Palosaari, T. Manninen, R. Toppila, and T. Kauppi, “Static strain aging of stabilized ferritic stainless steels,” *Metall. Ital.*, vol. 104, no. 9, pp. 25–28, 2012.

[35] A. Ekrami, “High temperature mechanical properties of dual phase steels,” *Mater. Lett.*, vol. 59, no. 16, pp. 2070–2074, 2005.

[36] L. P. Kubin, Y. Estrin, and C. Perrier, “On static strain ageing,” *Acta Metall. Mater.*, vol. 40, no. 5, pp. 1037–1044, 1992.

[37] A. van den Beukel, “Theory of the effect of dynamic strain aging on mechanical properties,” *Phys. Status Solidi*, vol. 30, no. 1, pp. 197–206, 1975.

[38] K. Cvetkovski, J. Ahlström, and B. Karlsson, “Monotonic and cyclic deformation of a high silicon pearlitic wheel steel,” *Wear*, vol. 271, no. 1–2, pp. 382–387, 2011.

[39] C.-C. Li and W. C. Leslie, “Effects of Dynamic Strain Aging on the Subsequent Mechanical Properties of Carbon Steels,” *Metall. Trans. A*, vol. 9A, no. December, pp. 1765–1775, 1978.

[40] S. L. Mannan, “Role of dynamic strain ageing in low cycle fatigue,” *Bull. Mater. Sci.*, vol. 16, no. 6, pp. 561–582, 1993.

[41] A. J. Wilkinson and D. Randman, “Determination of elastic strain fields and geometrically necessary dislocation distributions near nanoindents using electron back scatter diffraction,” *Philos. Mag.*, vol. 90, no. 9, pp. 1159–1177, 2010.

[42] T. Takahashi, D. Ponge, and D. Raabe, “Investigation of orientation gradients in pearlite in hypoeutectoid steel by use of orientation imaging microscopy,” *Steel Res. Int.*, vol. 78, no. 1, 2007.

[43] C. Moussa, M. Bernacki, R. Besnard, and N. Bozzolo, “About quantitative EBSD analysis of deformation and recovery substructures in pure Tantalum,” *IOP Conf. Ser. Mater. Sci. Eng.*, vol. 89, no. 1, p. 012038, 2015.

[44] S. I. Wright, M. M. Nowell, and D. P. Field, “A Review of Strain Analysis Using Electron Backscatter Diffraction,” *Microsc. Microanal.*, vol. 17, no. 03, pp. 316–329, 2011.

[45] K. Cvetkovski, “Influence of thermal loading on mechanical properties of railway wheel steels,” *Dep. Mater. Manuf. Technol.*, 2012.

[46] G. Vander Voort and A. Roosz, “Measurement of the interlamellar spacing of pearlite,” *Metallography*, vol. 17, pp. 1–17, 1984.